Electrical assessment of brownmillerite-type calcium ferrite materials obtained by proteic sol-gel route and by solid-state reaction using mollusk shells

Chrystian G. M. Lima[a], Allan J. M. Araújo[b,c], Rinaldo M. Silva[d], Rafael A. Raimundo[e], João P. F. Grilo[f,], Gabriel Constantinescu[f,*], Andrei V. Kovalevsky[f], Daniel A. Macedo[a,*]

[a] Materials Science and Engineering Postgraduate Program, UFPB, 58051-900 João Pessoa, Brazil

[b] Materials Science and Engineering Postgraduate Program, UFRN, 59078-970 Natal, Brazil

[c] Centre for Mechanical Technology and Automation, Mechanical Engineering Department, University of Aveiro, Aveiro, 3810-193, Portugal

[d] Department of Chemical Engineering, UFPB, 58051-900, Joao Pessoa, Brazil

[e] Mechanical Engineering Postgraduate Program, UFPB, 58051-900, João Pessoa, Brazil

[f] CICECO – Aveiro Institute of Materials, Department of Materials and Ceramic Engineering, University of Aveiro, 3810-193 Aveiro, Portugal

*Corresponding authors: gabriel.constantinescu@ua.pt (Gabriel Constantinescu), daniel.macedo@academico.ufpb.br (Daniel Macedo).

Abstract

In this work, brownmillerite-type calcium ferrite ($Ca_2Fe_2O_5$) ceramics were prepared by two distinct routes, namely by a proteic sol-gel synthesis using commercial flavorless gelatin, and by a solid-state reaction method using mollusk shells. XRD analyses revealed single phase brownmillerite-type calcium ferrites in both cases. SEM-EDS analysis of sintered $Ca_2Fe_2O_5$ ceramics revealed larger grain sizes for the samples prepared via the solid-state reaction. All samples possessed a p-type conduction mechanism, with the largest power factor of ~2 $\mu Wm^{-1} K^{-2}$ at 450 °C observed for the samples obtained via the solid state reaction. The charge transport mechanism was found to depend on the preparation route. The obtained results demonstrated that the proposed synthesis routes can be successfully employed for the preparation of single-phase brownmillerite-type materials.

Keywords: $Ca_2Fe_2O_5$; Proteic sol-gel synthesis; Solid-state reaction; Mollusk shells; Electrical properties

1. Introduction

The Seebeck effect is responsible for the direct conversion of temperature gradients into electricity, in certain functional materials. Some special technical ceramics are considered for thermoelectric (TE) applications at high temperatures, having a great potential for waste heat recovery, like, e. g., solid oxide fuel cells (SOFCs) [1]. Misfit layered p-type cobaltites such as $Na_xCoO_{2-\delta}$, $[Ca_2CoO_{3-\delta}]_{0.62}[CoO_2]$ ($Ca_3Co_4O_9$) and $[Bi_{0.87}SrO_2]_2[CoO_2]_{1.82}$ ($Bi_2Sr_2Co_{1.8}O_\delta$) have been broadly studied for their promising TE properties [2–4]. Another class of materials that has been investigated for TE applications is represented by brownmillerite oxides ($A_2B_2O_5$) [5]. Of these oxides types, literature reports on the calcium ferrites ($Ca_2Fe_2O_5$) are scarce [6–8]. Research groups/papers have reported several synthesis methods for preparing brownmillerite-type calcium ferrites, such as sol-gel [9], solid-state reaction [10–13], coprecipitation [13] and electrospinning [14], among others. Recently, our group successfully synthesized high-quality $[Ca_2CoO_{3-\delta}]_{0.62}[CoO_2]$ materials via two environmentally friendly routes and studied their TE properties [15]. The environmentally friendly methods consist in the use of mollusk shell powder, as a natural source of calcium carbonate, in the solid-state reaction [16], and in the use of commercial flavorless gelatin, as a low-cost precursor, in a proteic sol-gel synthesis [17], being a 'modified *Pechini* method' [18].

Materials which are considered promising for TE applications must simultaneously possess high electrical conductivity and Seebeck coefficient values, and low thermal conductivity [19]. Asenath-Smith *et al.* [6] reported thermal conductivity values of ~ 2 W/(m×K), for perovskite $Ca_2Fe_2O_5$ ceramics. The authors explain that the similarity of the thermal conductivity values of $Ca_2Fe_2O_5$ to the Ruddlesden-Popper phase implies the potential of the layered nature of brownmillerite-type compounds to reduce thermal conductivity through increased phonon scattering even if the material is composed of relatively light elements. This work aims to explore the effect of the preparation method on the electrical properties (electrical conductivity, Seebeck coefficient and power factor) at high temperatures in air, employing two alternative, low-cost, and environmentally friendly methods to obtain reactive calcium ferrite ceramic precursor powders for producing single phase ceramics with a brownmillerite-type structure.

2. Experimental

Single-phase $Ca_2Fe_2O_5$ (CFO) powders were obtained by two distinct methods, a solid-state reaction and a proteic sol-gel synthesis route. For the sake of simplicity, materials were labeled as CFO-M and CFO-G for the compounds obtained by milling and sol-gel synthesis route, respectively. For the proteic sol-gel method, gelatin was dissolved in distilled water at 50 °C and, subsequently, iron and calcium nitrates were added in stoichiometric amounts at 70 °C. In order to form a resin, the temperature was increased to 90 °C. A heat treatment was conducted at 300 °C for 2 h, which is related to the events of dehydration, nitrate decomposition and elimination of organic matter. Ca and Fe nitrates were purchased from Sigma-Aldrich. The solid-state reaction was performed by using mollusk shell powder and iron oxide (in stoichiometric amounts). Characterization of these mollusk shells can be found in a previous work [16]. The iron oxide was obtained from the proteic sol-gel synthesis using gelatin and iron nitrate (calcined at 600 °C). The materials were mixed/milled in alcohol medium at 400 rpm for 10 h, dried at 110 °C for 12 h and granulated through a 200-mesh sieve. The powders CFO-G and CFO-M were calcined at 900 °C for 2 h and pellets were sintered at 900 °C for 24 h.

Both powders were characterized by X-ray diffractometry (XRD-7000, Shimadzu ⟶ Cu-Kα) and field-emission scanning electron microscopy (FESEM, Carl Zeiss, Supra 35-VP Model). *Rietveld* refinement using Materials Analysis Using Diffraction (MAUD) software was performed. Inorganic Crystal Structure Database (ICSD) was used to obtain the crystal structures for refinement of the X-ray data. The microstructure of sintered pellets was studied by scanning electron microscopy coupled with energy dispersive spectroscopy (SEM-EDS, Hitachi SU-70). Apparent densities of the sintered ceramics were measured by the Archimedes' principle and the relative densities were determined from the ratio between the apparent densities and the theoretical density (4.01 g cm^{-3}).

Electrical conductivity and Seebeck coefficient measurements were simultaneously conducted on selected bar-shaped samples (~10 × 3 × 3 mm) of each type, in constant air flow, using the custom setup described in detail elsewhere [20], from 400 to 800°C, with a step of 50°C, using a steady-state technique. Freshly cut CFO-G and CFO-M samples were fixed inside a specially designed alumina sample chamber, placed in turn inside an atmosphere-controlled high-temperature furnace, one horizontally (σ, electrically connected in the setup with fine Pt wire, following a four-point probe DC technique arrangement and using an applied electric current, for a good use of Ohm's law) and the other vertically (α, subjected to a constant, discrete temperature gradient of ~14°C). The PF values were calculated from the α and σ values in each case, at each temperature step.

The high-temperature TE assessment of the final sintered ceramics is done by simultaneous electrical conductivity and Seebeck coefficient measurements in air, in a custom, 'home-made' experimental setup described elsewhere [20]. The activation energy values E_a for both parameters were calculated from the slopes of the linear fits of the respective $ln(\sigma T)$ vs. $1/T$ and α vs. 1/T (Arrhenius) plots (not shown), based on the models described in [6,21].

The XRD and TE coefficient plots were constructed using the OrginPro software, which was also used for the Ea calculations.

3. Results and Discussion

Figure 1 (a, c and e) displays the XRD patterns, refinement fitting results and difference of powders prepared by both presented methods. All patterns presented a single-phase oxide, indexed as Fe_2O_3 (Figure 1 (a)) and $Ca_2Fe_2O_5$ (Figure 1 (c and e), for CFO-M and CFO-G, respectively). Estimated lattice and structure parameters (from *Rietveld* refinement) of the calcined powders are shown in Table 1. Calcium ferrite samples were refined using the ICSD card number 88986 and iron oxide with the ICSD card number 15840. The brownmillerite-type calcium ferrite has orthorhombic symmetry with space group *Pnma* (no. 62), at room temperature, and the crystal structure of iron oxide (Fe_2O_3) is trigonal – *R-3cH* (no. 167). The lack of secondary phase and the obtention of very crystalline single-phase of CFO indicates that both processing routes can be considered as appropriate methods to obtain calcium ferrite with brownmillerite-type structure. Figure 1 (b, d and f) shows FESEM images of Fe_2O_3 and $Ca_2Fe_2O_5$ calcined particles. Higher agglomeration is noticeable in the solid-state reaction compared to the proteic sol-gel method, as also observed in a previous work [15]. The formation of a polymeric resin in the proteic sol-gel synthesis contributes to this fact [22]. On the other hand, aggregation of particles is observed in the CFO-G powder.

The brownmillerite mineral $Ca_2Fe_2O_5$ consists of alternating layers of corner-sharing FeO_6 octahedra and layers of FeO_4 tetrahedra, as illustrated in Figure 2. This structure is considered a perovskite with oxygen deficiency ordered along the [101] direction in alternate layers, which contributes to ionic conductivity [6,8,23].

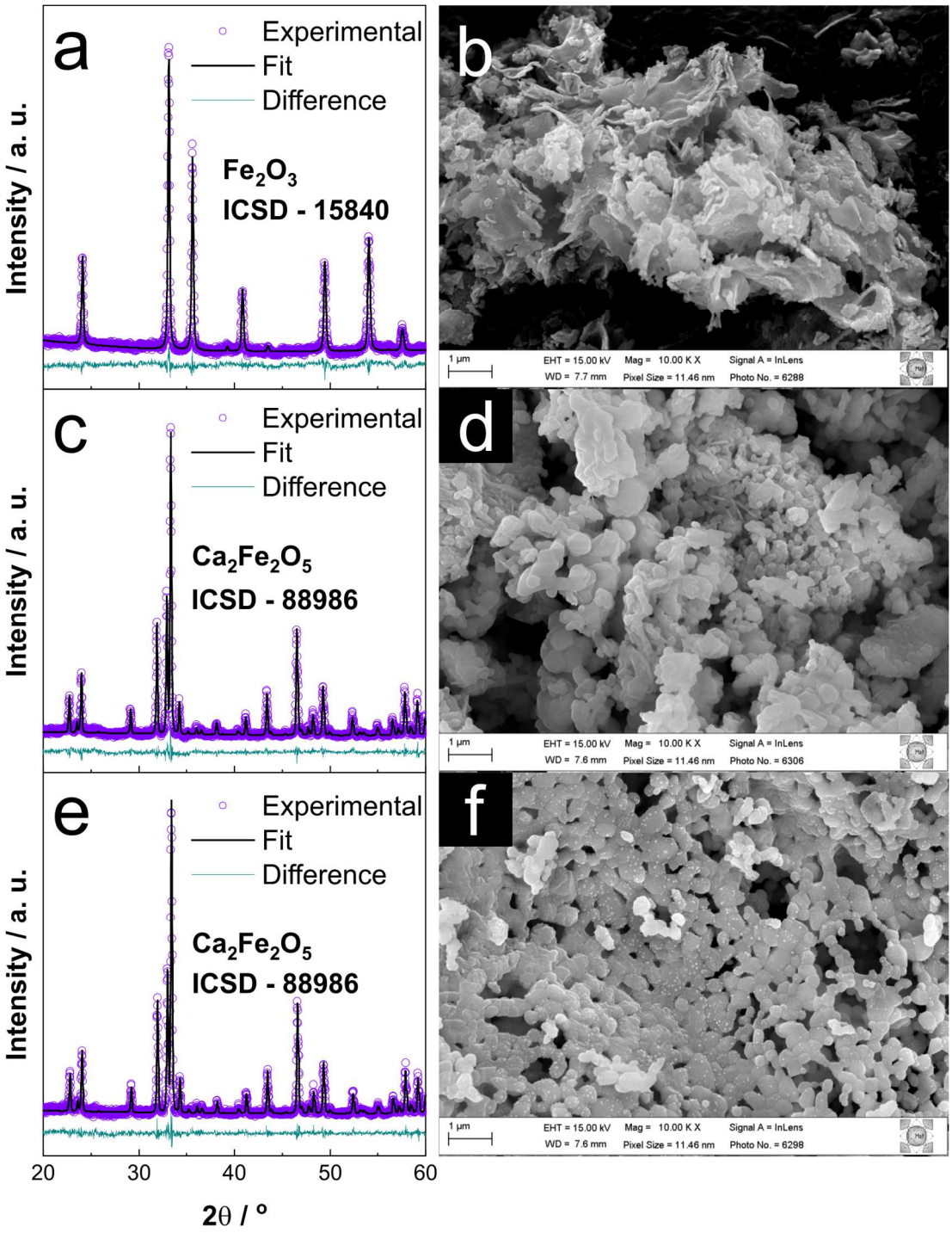

Figure 1. *Rietveld* refinement of the room-temperature XRD patterns and FESEM images of Fe_2O_3 particles (a, b), $Ca_2Fe_2O_5$ powders obtained by solid-state reaction (c, d) and by the proteic sol-gel method (e, f).

Table 1. Lattice and structure parameters for the Fe_2O_3 powder synthesized by proteic sol-gel route and calcium ferrite powders prepared by solid-state reaction using mollusk shells (CFO-M) and proteic sol-gel method (CFO-G). The chi-square (χ^2) values obtained evidence the good quality of the fit between the calculated and the experimental data [24].

Sample	Unit cell			Structure parameters					Agreement factors		
	a / Å	b / Å	c / Å	Atom	x	y	z	Site	R_{wp} / %	R_{exp} / %	χ^2
Fe_2O_3	5.0359	5.0359	13.7521	Fe1	0.00000	0.00000	0.35513	12c	10.68	10.44	1.02
				O1	0.31007	0.00000	0.25000	18e			
CFO-M	5.5980	14.7724	5.4266	Ca1	0.03066	0.10927	0.48163	8d	6.43	9.40	0.68
				Fe1	0.00000	0.00000	0.00000	4a			
				Fe2	-0.06590	0.25000	-0.05988	4c			
				O1	0.24824	-0.01353	0.28256	8d			
				O2	0.05494	0.14977	0.01701	8d			
				O3	0.85155	0.25000	0.59564	4c			
CFO-G	5.5967	14.7674	5.4256	Ca1	0.03091	0.10842	0.48392	8d	6.99	9.45	0.73
				Fe1	0.00000	0.00000	0.00000	4a			
				Fe2	-0.06281	0.25000	-0.06014	4c			
				O1	0.26182	-0.01306	0.29000	8d			
				O2	0.05753	0.14780	0.02255	8d			
				O3	0.84957	0.25000	0.59751	4c			

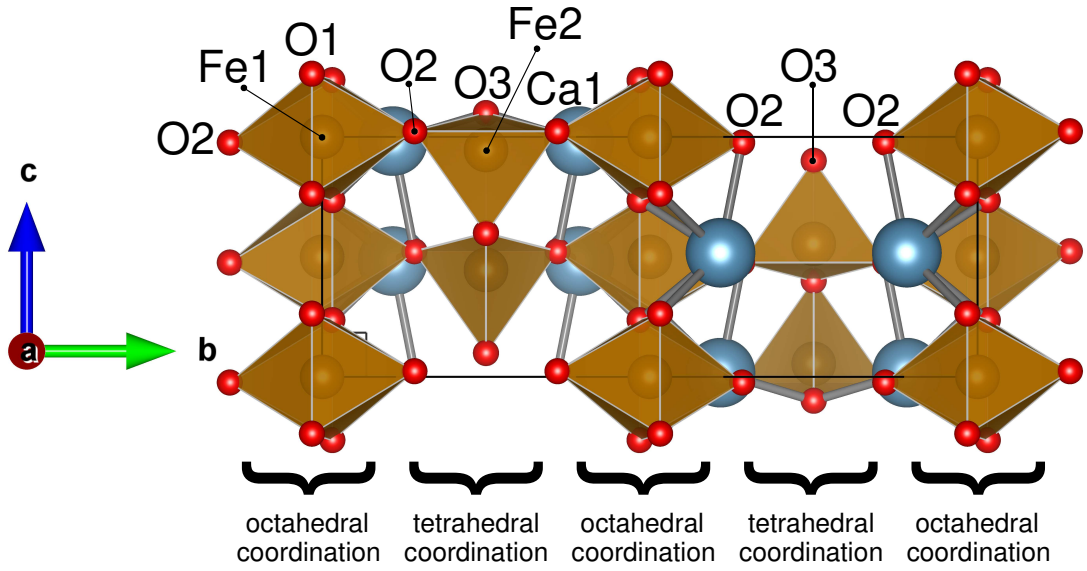

Figure 2. Illustration of the brownmillerite structure of $Ca_2Fe_2O_5$ based on the ICSD 88986 used to refine the CFO-M and CFO-G samples.

SEM-EDS images of ceramics sintered at 900 ºC are shown in Figure 3 (relative density of about 62 % in both samples). The ceramics retain sub-micron grain size, provided by the high-quality precursor powders. While the grain shape is similar, a noticeable difference in the grain size (Figure 3 (a, b)) is likely provided by more coarse mollusk shell powder as compared to the precursor produced

by a proteic sol-gel synthesis. EDS mapping (Figure 3 (c, d)) reveals the homogeneous distribution of Ca and Fe elements in both samples.

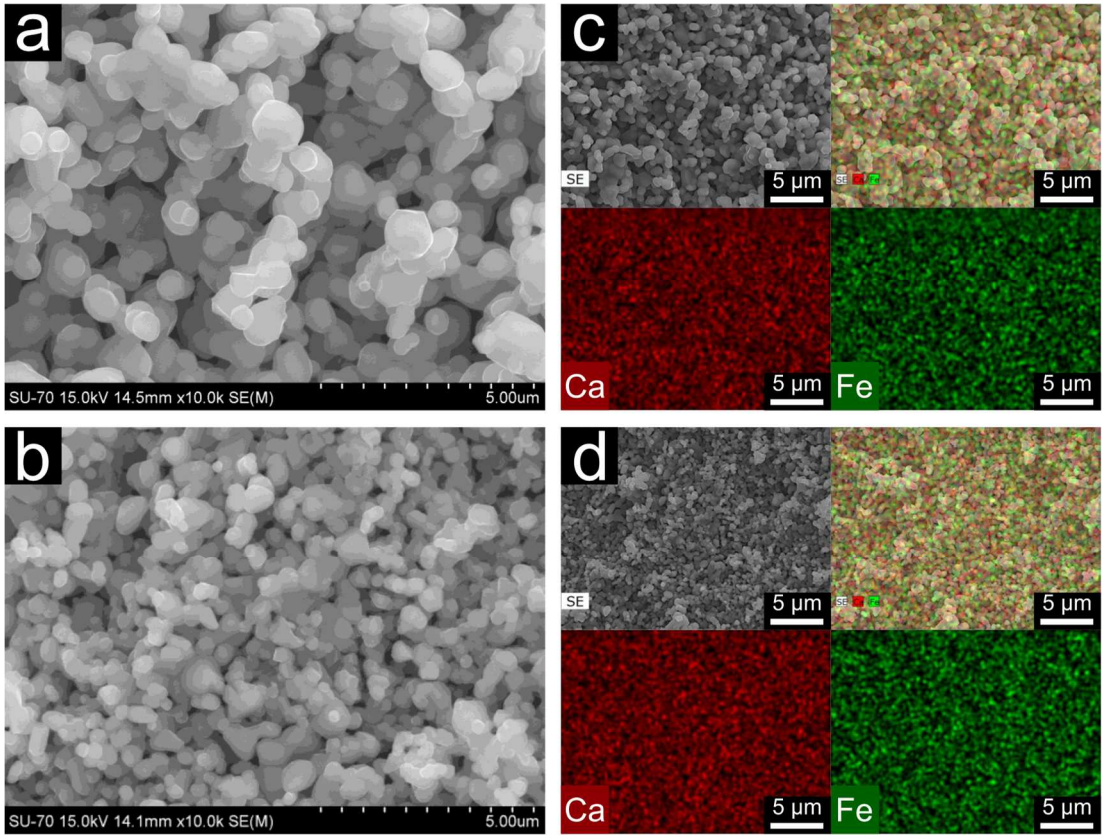

Figure 3. SEM images of the CFO-M and CFO-G pellets (a and b, respectively) and their EDS mapping images (c and d, respectively). Insets in c and d are self-explanatory.

Figure 4 depicts the temperature dependence of the Seebeck coefficient for the the $Ca_2Fe_2O_5$ ceramics fabricated by the two synthetic methods. Positive Seebeck values confirm a dominating p-type conduction mechanism (Figure 4). However, significant differences are observed in the temperature dependence of the Seebeck coefficient. This indicates that the selected preparation methods affect the charge transport mechanism in brownmillerite, since usually the Seebeck coefficient does not depend on the microstructure.

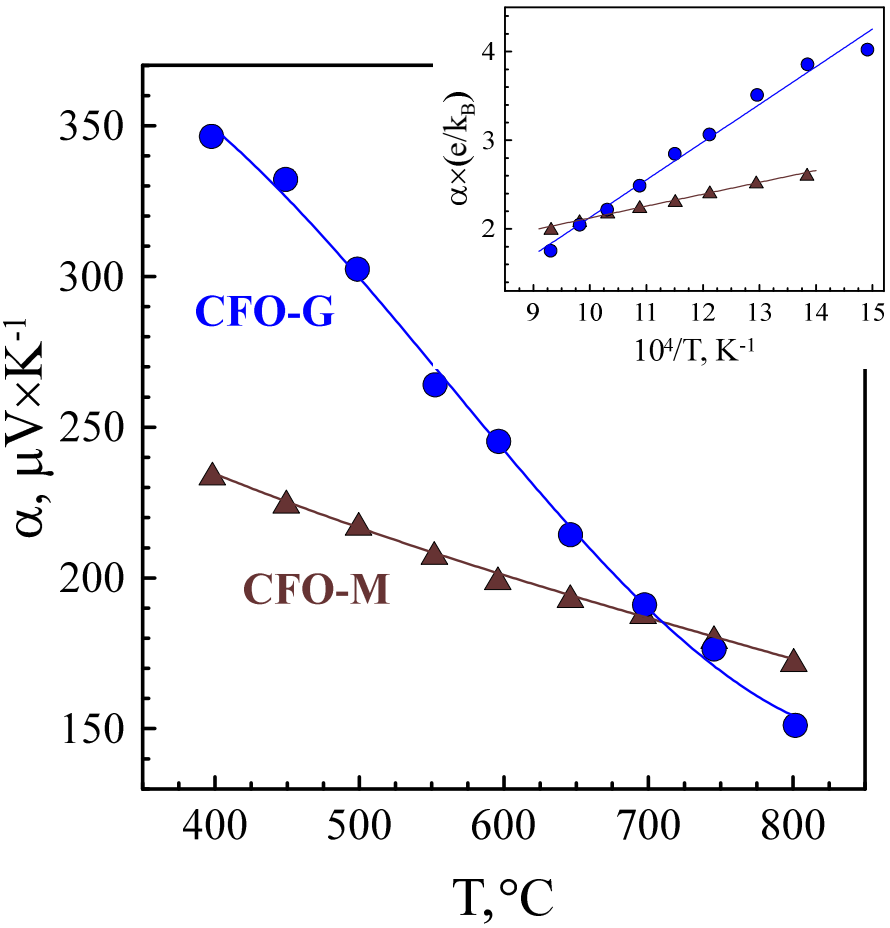

Figure 4. Seebeck coefficient of $Ca_2Fe_2O_5$ ceramics obtained via solid state reaction (CFO-M) and by a proteic sol-gel method (CFO-G). The inset shows Arrhenius plots used for calculating the activation energy.

Electronic conduction mechanism dominates the total conductivity of CFO ceramics due to the two-dimensional nature of brownmillerite-type structures [8]. Shaula *et al.* [8] reported a low ionic conductivity of CFO ceramics when compared to ferrite-based perovskites ($SrFe(Al)O_{3-\delta}$ or $Sr(La)Fe(Ga)O_{3-\delta}$) and explained this behavior based on the low concentration of oxygen vacancies in the octahedra layers of the brownmillerite structure. Figure 5 shows Arrhenius plots of the electrical conductivity, using a representation consistent with a polaron conduction model [6,21]:

$$\sigma T = \sigma_0 \exp\left(-\frac{E_\sigma}{k_B T}\right) \qquad \text{(Eq. 1)}$$

where E_σ is the activation energy of polaron conduction, k_B is the Boltzmann constant.

The conductivity of CFO-M is 2.4-7.3 times higher than for CFO-G (Figure 5), the difference is decreasing on heating, likely provided by the same effects as the crossover of Seebeck coefficient at ~720 ºC.

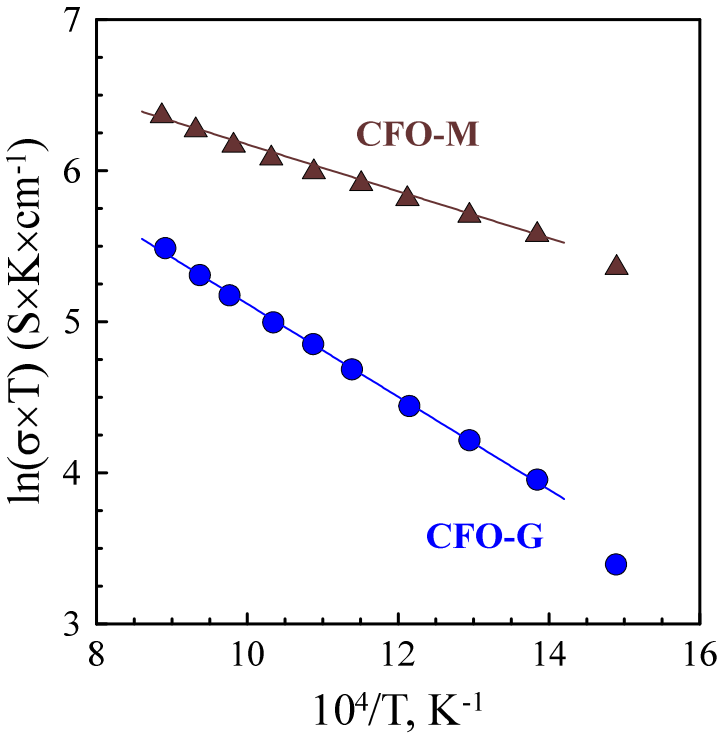

Figure 5. Electrical conductivity (Arrhenius plots) of $Ca_2Fe_2O_5$ ceramics obtained via solid state reaction (CFO-M) and by a proteic sol-gel method (CFO-G).

More guidelines can be obtained from the analysis of calculated values of the activation energies, depicting several similar mechanisms described in [6]. The activation energy for Seebeck coefficient (E_α) can be calculated from the (Eq. 2) [6]:

$$\alpha = \frac{k_B}{e}\left(\frac{E_\alpha}{k_B T} + \frac{S_v}{k_B}\right) \qquad \text{(Eq.2)}$$

where S_v is vibrational(transport) entropy of the polaron. At 450-800 ºC, the E_σ values for CFO-M and CFO-G samples amount to 0.134 and 0.265 eV, correspondingly, being comparable to those obtained in [6]. Both samples also show linear behaviour of the Seebeck coefficient with inverse temperature (inset in Fig. 4). Corresponding activation energies E_α amount to 0.115 and 0.366 eV for CFO-M and CFO-G samples, correspondingly. The difference (E_σ–E_α) represents the binding energy of the polaron [6], and the case $E_\alpha < E_\sigma$ for CFO-M illustrates temperature-activated mobility consistent with polaron conduction, in agreement with the results obtained in [6]. A striking observation is that the E_α values are notably higher than E_σ for the CFO-G sample, indicating that the preparation route affects the conduction mechanism. The classical relation $\sigma = n \times e \times \mu$ suggests that the variation of the conductivity

with temperature is contributed by the corresponding variations of the charge carrier concentration (n) and mobility (μ). In turn, the Seebeck coefficient is directly related only to the charge carrier concentration. The more pronounced temperature-activated character of the Seebeck coefficient should be compensated by an opposite tendency in the mobility behaviour, to result in the observed moderate temperature dependence of the electrical conductivity. Thus, the results obtained for CFO-G apparently evidence the contribution of the broadband conduction mechanism for this sample, with the charge carrier mobility presumably decreasing on heating. The origin of such a change in the conductivity mechanism is likely related to the specific effects provided by the localized states at the grain boundaries, as it might be expected for nanosized grain structure in the case of proteic sol-gel synthesis route. However, additional studies including Hall effect measurements, impedance spectroscopy and TEM analysis are required to understand better the observed effects.

As a result, the power factor is significantly affected by the involved preparation methods (Figure 6). The effect is mainly provided by the conductivity difference, which is likely related to more pronounced grain boundary scattering of the charge carriers in the case of CFO-G.

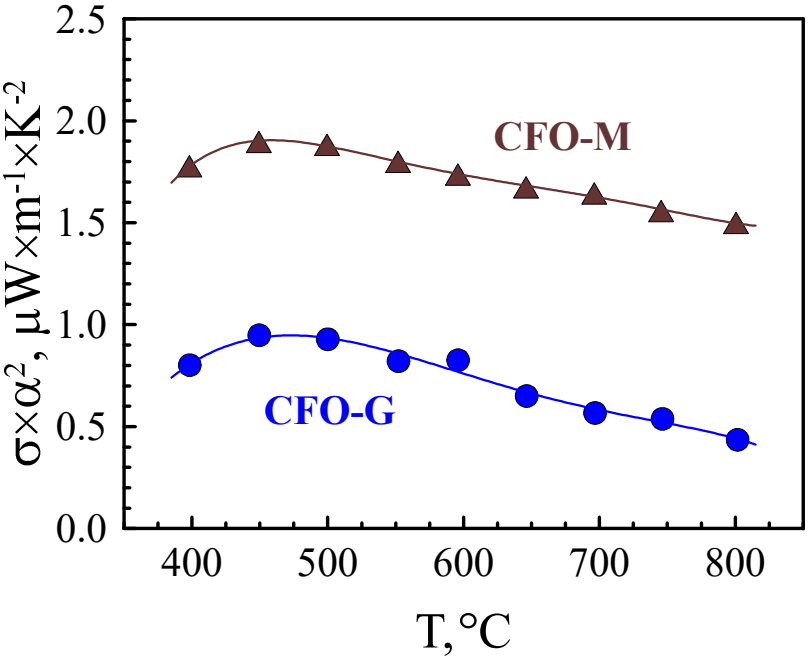

Figure 6. Power factor of $Ca_2Fe_2O_5$ ceramics obtained via solid state reaction (CFO-M) and by a proteic sol-gel method (CFO-G).

Although the overall electrical performance is too low for considering $Ca_2Fe_2O_5$ for thermoelectric applications, the work demonstrates, for the first time, the possibility of fabricating brownmillerite-type structure material by using mollusk shells in a solid-state reaction and gelatin as

a low-cost precursor by a proteic sol-gel route. Therefore, these routes are competitive to be used in future works with, e. g., substituted calcium ferrite, in order to improve the electrical performance, as reported for SOFC cathode applications [25]. Secondly, more pronounced temperature-activated behaviour of the Seebeck coefficient of the material prepared via proteic sol-gel route, as compared to the electrical conductivity, suggests the contribution of the band conduction mechanism, which potentially may result in better electrical performance, promoted by suitable substitution approaches.

4. Conclusions

Pure $Ca_2Fe_2O_5$ ceramic precursors were successfully prepared by a proteic sol-gel synthesis method and by a solid-state reaction method using powdered mollusk shells. The electrical assessment of sintered ceramics showed that the involved methods affect the charge transport mechanisms, with different contribution from charge carrier generation and temperature-activated mobility. As a result, the electronic transport mechanism is apparently contributed by the band conduction in the material prepared via proteic sol-gel synthesis, while polaron hopping mechanism is predominant for ceramics prepared via solid-state reaction. Both synthesis methods are competitive routes for the preparation of materials with brownmillerite-type structure.

Conflict of interest

None.

Acknowledgements

This study was financed by CAPES/Brazil, Finance Code 001. Allan Araújo, João Grilo and Daniel Macedo acknowledge CNPq/Brazil (200439/2019-7, 431428/2018-2 and 309430/2019-4). This research was also funded by the projects REMOTE (POCI-01-0145-FEDER-031875), CICECO–Aveiro Institute of Materials (UIDB/50011/2020 and UIDP/50011/2020), financed by COMPETE 2020 Program and National Funds through the FCT/MEC and, when applicable, co-financed by FEDER under the PT2020 Partnership Agreement.

References

[1] H. Zhang, H. Xu, B. Chen, F. Dong, M. Ni, Two-stage thermoelectric generators for waste

heat recovery from solid oxide fuel cells, Energy. 132 (2017) 280–288. https://doi.org/10.1016/j.energy.2017.05.005.

[2] M.A. Madre, F.M. Costa, N.M. Ferreira, A. Sotelo, M.A. Torres, G. Constantinescu, S. Rasekh, J.C. Diez, Preparation of high-performance $Ca_3Co_4O_9$ thermoelectric ceramics produced by a new two-step method, J. Eur. Ceram. Soc. 33 (2013) 1747–1754. https://doi.org/10.1016/j.jeurceramsoc.2013.01.029.

[3] K. Rubešová, T. Hlásek, V. Jakeš, S. Huber, J. Hejtmánek, D. Sedmidubský, Effect of a powder compaction process on the thermoelectric properties of $Bi_2Sr_2Co_{1.8}O_x$ ceramics, J. Eur. Ceram. Soc. 35 (2015) 525–531. https://doi.org/10.1016/j.jeurceramsoc.2014.08.037.

[4] K. Fujita, T. Mochida, K. Nakamura, High-temperature thermoelectric properties of $Na_xCoO_{2-\delta}$ single crystals, Jpn. J. Appl. Phys. 40 (2001) 4644–4647. https://doi.org/10.1143/JJAP.40.4644.

[5] W. Kobayashi, A. Satake, I. Terasaki, Thermoelectric properties of the brownmillerite oxide $Ca_{2-y}La_yCo_{2-x}Al_xO_5$, Jpn. J. Appl. Phys. 41 (2002) 3025–3028. https://doi.org/10.1143/JJAP.41.3025.

[6] E. Asenath-Smith, I.N. Lokuhewa, S.T. Misture, D.D. Edwards, p-Type thermoelectric properties of the oxygen-deficient perovskite $Ca_2Fe_2O_5$ in the brownmillerite structure, J. Solid State Chem. 183 (2010) 1670–1677. https://doi.org/10.1016/j.jssc.2010.05.016.

[7] H.D. Zhou, J.B. Goodenough, Electronic behavior of three oxygen non-stoichiometric Fe_{4+}/Fe_{3+} oxoperovskites, J. Solid State Chem. 178 (2005) 3679–3685. https://doi.org/10.1016/j.jssc.2005.09.020.

[8] A.L. Shaula, Y. V. Pivak, J.C. Waerenborgh, P. Gaczyñski, A.A. Yaremchenko, V. V. Kharton, Ionic conductivity of brownmillerite-type calcium ferrite under oxidizing conditions, Solid State Ionics. 177 (2006) 2923–2930. https://doi.org/10.1016/j.ssi.2006.08.030.

[9] M. Vanags, A. Spule, K. Gruškeviča, S. Vihodceva, A. Tamm, S. Vlassov, A. Šutka, Sol-gel auto-combustion synthesis of $Ca_2Fe_2O_5$ brownmillerite nanopowders and thin films for advanced oxidation photoelectrochemical water treatment in visible light, J. Environ. Chem. Eng. 7 (2019) 103224. https://doi.org/10.1016/j.jece.2019.103224.

[10] B.F. Amorim, M.A. Morales, F. Bohn, A.S. Carriço, S.N. De Medeiros, A.L. Dantas, Synthesis of stoichiometric $Ca_2Fe_2O_5$ nanoparticles by high-energy ball milling and thermal annealing, Phys. B Condens. Matter. 488 (2016) 43–48. https://doi.org/10.1016/j.physb.2016.01.029.

[11] C.B. Azzoni, M.C. Mozzati, V. Massarotti, D. Capsoni, M. Bini, New insights into the magnetic properties of the $Ca_2Fe_2O_5$ ferrite, Solid State Sci. 9 (2007) 515–520. https://doi.org/10.1016/j.solidstatesciences.2007.04.013.

[12] L.A. Isupova, S. V. Tsybulya, G.N. Kryukova, A.A. Budneva, E.A. Paukshtis, G.S. Litvak, V.P. Ivanov, V.N. Kolomiichuk, Y.T. Pavlyukhin, V.A. Sadykov, Mechanochemical synthesis and catalytic properties of the calcium ferrite $Ca_2Fe_2O_5$, Kinet. Catal. 43 (2002) 122–129. https://doi.org/10.1023/A:1014217716883.

[13] M. Ismail, W. Liu, M.S.C. Chan, M.T. Dunstan, S.A. Scott, Synthesis, Application, and

Carbonation Behavior of $Ca_2Fe_2O_5$ for Chemical Looping H_2 Production, Energy and Fuels. 30 (2016) 6220–6232. https://doi.org/10.1021/acs.energyfuels.6b00631.

[14] X. Xu, S. Li, X. Wang, Y. Ma, X. Wang, K. Gao, Fabrication and characterization of $Ca_2Fe_2O_5$ nanofibers photocatalyst by sol-gel assisted electrospinning at low-temperature, Mater. Lett. 143 (2015) 75–79. https://doi.org/10.1016/j.matlet.2014.12.065.

[15] A.A. Emerenciano, A.J.M. Araújo, J.P.F. Grilo, D.A. Macedo, S. Rasekh, A. V Kovalevsky, C.A. Paskocimas, R.M. Nascimento, Environmentally friendly synthesis methods to obtain the misfit $[Ca_2CoO_{3-\delta}]_{0.62}[CoO_2]$ thermoelectric material, Mater. Lett. 254 (2019) 286–289. https://doi.org/10.1016/j.matlet.2019.07.053.

[16] E.B.G.A. Fulgêncio, K.P. V Melo, R.M. Silva, J.P.F. Grilo, V. Caignaert, M.R. Cesário, L.F.A. Campos, D.A. Macedo, Misfit Ca-cobaltite from a mixture of mollusk shells and cobalt oxide as potential SOFC cathode material, Ceram. Int. 43 (2017) 9564–9567. https://doi.org/10.1016/j.ceramint.2017.04.099.

[17] L.S. Ferreira, T.R. Silva, V.D. Silva, T.A. Simões, A.J.M. Araújo, M.A. Morales, D.A. Macedo, Proteic sol-gel synthesis, structure and battery-type behavior of Fe-based spinels (MFe_2O_4, M = Cu, Co, Ni), Adv. Powder Technol. 31 (2020) 604–613. https://doi.org/10.1016/j.apt.2019.11.015.

[18] M.P. Pechini, Method of preparing lead and alkaline earth titanates and niobates and coating method using the same to form a capacitor, US3330697A, 1967.

[19] G. Constantinescu, A.R. Sarabando, S. Rasekh, D. Lopes, S. Sergiienko, P. Amirkhizi, J.R. Frade, A. V. Kovalevsky, Redox-promoted tailoring of the high-temperature electrical performance in $Ca_3Co_4O_9$ thermoelectric materials by metallic cobalt addition, Materials (Basel). 13 (2020) 1060. https://doi.org/10.3390/ma13051060.

[20] A.V. V. Kovalevsky, A.A.A. Yaremchenko, S. Populoh, A. Weidenkaff, J.R.R. Frade, Enhancement of thermoelectric performance in strontium titanate by praseodymium substitution, J. Appl. Phys. 113 (2013) 053704. https://doi.org/10.1063/1.4790307.

[21] R.J.D. Tilley, Defects in Solids, Encycl. Inorg. Chem. (2018). https://doi.org/10.1002/9781119951438.eibc0058.pub2.

[22] Y.F. Zhang, J.X. Zhang, Q.M. Lu, Q.Y. Zhang, Synthesis and characterization of $Ca_3Co_4O_9$ nanoparticles by citrate sol-gel method, Mater. Lett. 60 (2006) 2443–2446. https://doi.org/10.1016/j.matlet.2006.01.013.

[23] I.A. Leonidov, V.L. Kozhevnikov, M. V Patrakeev, E.B. Mitberg, K.R. Poeppelmeier, High-temperature electrical conductivity of $Sr_{0.7}La_{0.3}FeO_{3-\delta}$, Solid State Ionics. 144 (2001) 361–369. https://doi.org/10.1016/S0167-2738(01)00978-X.

[24] H.M. Rietveld, A profile refinement method for nuclear and magnetic structures, J. Appl. Crystallogr. 2 (1969) 65–71. https://doi.org/10.1107/S0021889869006558.

[25] V. Cascos, R. Martínez-Coronado, J.A. Alonso, M.T. Fernández-Díaz, Structural and electrical characterization of the Co-doped $Ca_2Fe_2O_5$ brownmillerite: Evaluation as SOFC - cathode materials, Int. J. Hydrogen Energy. 40 (2015) 5456–5468. https://doi.org/10.1016/j.ijhydene.2015.01.067.